

Phonon thermal Hall effect in charge-compensated topological insulators

Rohit Sharma,^{1,*} Mahasweta Bagchi,¹ Yongjian Wang,¹ Yoichi Ando,¹ and Thomas Lorenz^{1,†}

¹*II. Physikalisches Institut, Universität zu Köln, Zùlpicher Str. 77, 50937 Köln, Germany*

(Dated: January 9, 2024)

From a systematic study of thermal and charge transport in various single crystals of compensated topological insulators we identify the evolution of a large low-temperature thermal Hall effect as a characteristic common feature. In order to separate phononic and electronic contributions in the measured longitudinal and transverse thermal conductivity, the electronic contributions are estimated from corresponding electrical resistivity and Hall effect measurements on the same samples by using the Wiedemann-Franz law. As may be expected for charge-compensated topological insulators the longitudinal thermal conductivity is phonon-dominated in all samples. However, we also find a pronounced field-linear thermal Hall effect that becomes most pronounced in the low-temperature range, where all samples are good electrical insulators. This indicates an underlying phononic mechanism of the thermal Hall effect and in this respect the topological insulators resemble other, mainly ionic, insulators, which have been reported to show a phonon-induced thermal Hall effect, but its underlying phononic mechanism remains to be identified. Our observation of a comparable thermal Hall ratio in topological insulators supports a theoretical scenario that explains a thermal Hall effect through skew scattering on charged impurities.

Thermal Hall Effect (THE) has gained significant scientific interest due to its unique ability to explore various excitations, like electrons, phonons, magnons and more exotic excitations like Majorana particles[1]. This sets it apart from the charge Hall effect, which only provides insights into mobile charged excitations, such as electrons. THE is the transverse temperature difference (ΔT_y) that emerges along the y axis when a heat current (J) and a magnetic field (H) are applied along the x and z axes, respectively. If charged particles contribute to the heat transport a finite THE is naturally expected from the Lorentz force and the corresponding heat and charge conductivities can be related via the Wiedemann-Franz law. However, despite the absence of charged carriers, insulators can also exhibit a THE as was first observed in paramagnetic $\text{Tb}_3\text{Ga}_5\text{O}_{12}$ [2]. This observation prompted theoretical discussions considering Raman-type interactions between large spins and phonons, the Berry curvature of phonon bands, and skew scattering of phonons by superstoichiometric Tb^{3+} ions [3–5]. Another source of THE in magnetic insulators is associated with the Berry curvature of magnon bands generated by the Dzyaloshinskii-Moriya interaction [6–9].

Subsequently, phonon-induced THE have been detected in various materials, such as multiferroic materials like $\text{Fe}_2\text{Mo}_3\text{O}_8$ [10], cuprate superconductors [11, 12], phonon glass systems like $\text{Ba}_3\text{CuSb}_2\text{O}_9$ [13], Mott insulators [14], the metallic spin-ice material $\text{Pr}_2\text{Ir}_2\text{O}_7$ [15], and the antiferromagnetic insulator Cu_3TeO_6 [16]. Remarkably, even non-magnetic SrTiO_3 exhibits a substantial phonon-induced THE that has been attributed to the presence of antiferrodistortive structural domains [17], and this THE is suppressed in isotopically substituted

$\text{SrTi}^{18}\text{O}_3$ [18] and Ca-doped samples [19]. A phonon-induced THE has been identified in elemental black phosphorus [20], another non-magnetic material, where the coupling of phonons with magnetic fields has been connected to anisotropic charge distribution. Theoretically two proposals for phonon induced THE have been put forward. On the one hand, intrinsic mechanisms consider a phonon THE arising from factors like Berry curvature in phonon bands [4], phonon scattering due to collective fluctuations [21], or interactions between phonons and other quasi-particles like magnons [22, 23]. On the other hand, extrinsic mechanisms rely on effects of phonon scattering by impurities or defects [24–26]. Despite intensive research, the exact origins of phonon-induced THE remain elusive. This highlights the importance of exploring various material classes, especially beyond oxide-based ionic insulators.

Here, we report the discovery of a large phonon-related THE in a series of $\text{Bi}_{2-x}\text{Sb}_x\text{Te}_{3-y}\text{Se}_y$ samples that belong to a different class of non-magnetic, insulating materials known as compensated three dimensional (3D) topological insulators (TIs). 3D TIs are characterized by an insulating bulk band structure in combination with gapless (conducting) surface states that arise from a non-trivial topology of the underlying wave functions [27]. Often, however, real TI materials are rather conducting due to defect-induced charge carriers and bulk insulating behavior is only reached by a specific compensation of donor and acceptor atoms [28]. From thermal and electrical transport measurements we identify a large THE as a common feature of several bulk insulating TIs. In a field of 14 T, large thermal Hall ratios $\kappa_{xy}/\kappa_{xx} \simeq -10^{-3}$ are reached and hardly vary over the low-temperature insulating phases. This compares well to the results obtained on many of the above mentioned insulators, see [16], and is in line with a recent theoretical proposal of a phonon THE arising from charged defects in (nonmagnetic) insulators [26].

* sharma@ph2.uni-koeln.de

† tl@ph2.uni-koeln.de

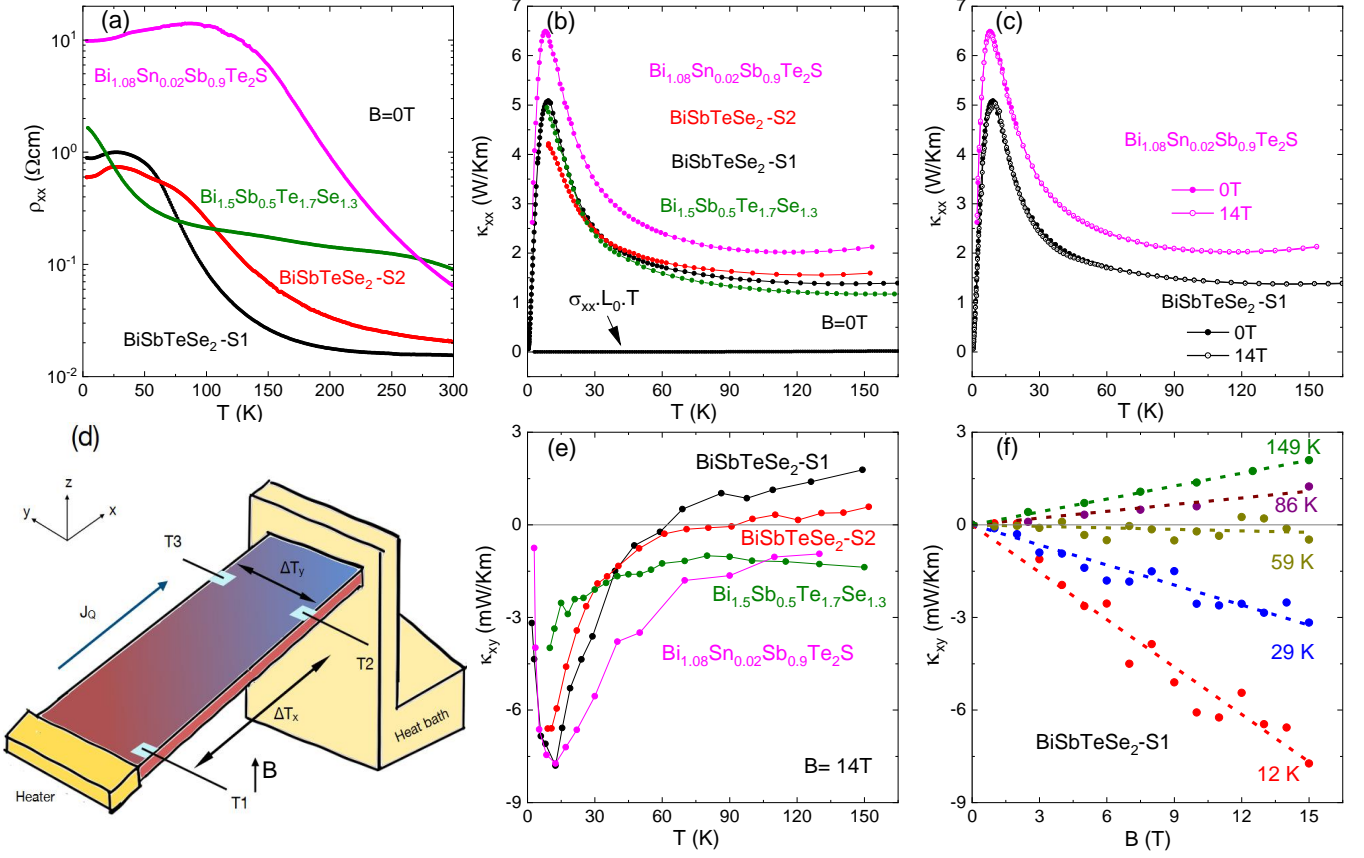


FIG. 1. Temperature dependence of (a) electrical resistivity ρ_{xx} and of (b) thermal conductivity κ_{xx} of various charge compensated topological insulators. The flat black line close to zero in (b) represents a negligible charge-carrier contribution $\kappa_{xx}^{el} = \sigma_{xx}L_0T$ estimated via the Wiedemann-Franz law for the sample BiSbTeSe₂-S1 with the lowest resistivity $\rho_{xx} = 1/\sigma_{xx}$. This reveals that κ_{xx} is phonon dominated for all samples and is further confirmed in (c) showing the magnetic-field independence of κ_{xx} . (d) Schematic setup to measure κ_{xx} and κ_{xy} from the longitudinal and transverse temperature differences ($\Delta T_x = T_1 - T_2$, $\Delta T_y = T_2 - T_3$) induced by a heat current $J_Q \parallel x$ in a magnetic field $H \parallel z$. (e) Temperature-dependent κ_{xy} in a magnetic field $\mu_0 H = 14$ T. For each sample, $\kappa_{xy}(T)$ was obtained from linear fits of field-antisymmetrized data measured at constant temperatures as is exemplarily shown in (f).

Single crystals of compensated TIs were grown from a melt of high-purity elements Bi, Sb, Te, Se, S, and Sn, using a modified Bridgman method in a sealed quartz-glass tube, as described in [28]. Freshly cleaved thin flakes were cut to rectangular shape to measure the longitudinal (ρ_{xx}) and Hall resistivities (ρ_{yx}) in a standard 6-point geometry using a DC current source and two nanovoltmeters at stabilized temperatures and discrete magnetic fields between ± 14 T. The same samples were used for measuring the longitudinal (κ_{xx}) and Hall (κ_{xy}) thermal conductivities using a steady-state 1-heater 3-thermometer method under high-vacuum conditions, as sketched in Fig. 1. A 10 k Ω RuO₂ chip resistor at one end of the sample was used to induce a heat current $J_Q = RI^2$ that results in longitudinal $\Delta T_x = T_1 - T_2$ and transverse $\Delta T_y = T_3 - T_2$ temperature differences. Up to about 100 K, $T_{1,2,3}$ were measured with Cernox sensors (CX1030) and, additionally, ΔT_x and ΔT_y were measured with constantan-chromel thermocouples in separate runs from about 30 to 200 K. Gold wires were con-

tacted to the sample with silver paste and were either connected to a commercial PPMS puck (Quantum Design) for the electrical measurements, or connected to the respective temperature sensors of different home-built setups for heat transport measurements. In order to eliminate the misalignment of the transverse contacts, the Hall voltage U_H or temperature difference ΔT_H were obtained by antisymmetrization of the respective raw data measured in $\pm B$, e.g. $U_H(B) = (U_y(+B) - U_y(-B))/2$. The thermal Hall conductivity is then obtained as $\kappa_{xy} = (\Delta T_H / \Delta T_x)(l/w)\kappa_{xx}$ with longitudinal thermal conductivity $\kappa_{xx} = (J_Q / \Delta T_x)(l/wt)$, distance l between the longitudinal contacts, sample width w , and thickness t . Analogously, the electrical resistivities are given by $\rho_{xx} = (U_{xx} / I_x)(wt/l)$ and $\rho_{yx} = (U_H / I_x)$, and the electrical Hall conductivity is $\sigma_{xy} = \rho_{yx} / (\rho_{xx}^2 + \rho_{yx}^2)$.

Figure 1(a) shows the longitudinal electrical resistivity of four TI samples. Two of them have the same composition BiSbTeSe₂ and show a very similar $\rho_{xx}(T)$ characterized by a temperature-activated behavior above 100 K

that turns into a low-temperature plateau. This is typical for this type of charge-compensated TIs and has been analyzed in detail previously [28]. Arrhenius fits $\rho_{xx} \propto \exp(\Delta/k_B T)$ yield activation energies around 35 meV in good agreement with the previous results, whereas a larger activation energy of 136 meV and an overall enhanced resistivity is found in $\text{Bi}_{1.08}\text{Sn}_{0.02}\text{Sb}_{0.9}\text{Te}_2\text{S}$ reflecting the higher degree of compensation in this type of TI material [29]. In contrast, neither the activated behavior nor the low-temperature plateau are well pronounced in $\rho_{xx}(T)$ of $\text{Bi}_{1.5}\text{Sb}_{0.5}\text{Te}_{1.7}\text{Se}_{1.3}$, indicating more disorder and a weaker degree of charge-carrier compensation in this sample.

The longitudinal thermal conductivity κ_{xx} varies little between the four samples, as is shown in Fig. 1(b). The peaks around 10 K are typical for phonon heat transport and result from the opposite temperature dependences of phonon heat capacity and phonon mean-free path which, respectively, increase and decrease with increasing temperature. In the related mother compounds Bi_2Se_3 and Bi_2Te_3 significantly higher κ_{xx} peaks of ~ 35 W/Km are observed [30, 31], whereas Sb_2Te_3 has a peak of ~ 20 W/Km that decreases to 6–8 W/Km when Sb is replaced by a few % of V [32]. The strong variation of the peak values is naturally attributed to the maximum phonon mean free path that sensitively depends on disorder effects, which vary with the composition and generally increase with the number of different constituents. Above 100 K, the κ_{xx} of our samples are only very weakly temperature dependent and lie in the range between 1–2 W/Km, which compares well with the values that are reached above about 200 K in the binary mother compounds [30–32].

Apart from the phonons, mobile charge carriers also contribute to the overall heat transport. The electronic contribution κ_{xx}^{el} to the heat transport can be estimated from the measured electrical conductivity σ_{xx} by using the Wiedemann-Franz law $\kappa_{xx}^{el} = L_0 \sigma_{xx} T$ with temperature T and Lorenz number $L_0 \approx 2.44 \times 10^{-8} \text{ V}^2\text{K}^{-2}$. In Fig. 1(b), the obtained electronic κ_{xx}^{el} is exemplarily included for the BiSbTeSe_2 -S1, but even for this best conducting sample κ_{xx}^{el} remains 2 orders of magnitude below the measured κ_{xx} over the entire temperature range. Thus, we can safely conclude that the thermal conductivity in all our samples is phonon dominated and this is further verified by the fact that κ_{xx} varies by less than 2% in a magnetic field of 14 T in all samples, as shown for two of them in Fig. 1(c).

Having established that κ_{xx} is fully phonon dominated, we direct our attention to κ_{xy} , which is sizeable and shows a linear magnetic-field dependence $\kappa_{xy} \propto B$ at constant T for all samples over the entire temperature range. Representative $\kappa_{xy}(B, T)$ curves are displayed in Fig. 1(f) for one sample and the other data sets are shown in the appendix. From linear fits of the $\kappa_{xy}(B)$ curves, we derive the temperature dependent $\kappa_{xy}(T)$ in a field of 14 T that is compared for all four samples in Fig. 1(e). At higher temperature, the sign of κ_{xy} is sam-

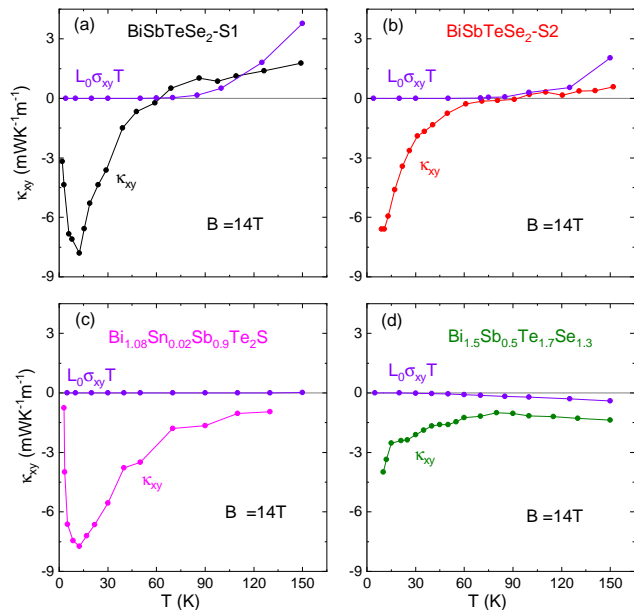


FIG. 2. Temperature dependent κ_{xy} data from Fig. 1(e) in comparison to the charge-carrier contributions $\kappa_{xy}^{el} = \sigma_{xy} L_0 T$ estimated via the Wiedemann-Franz law from the electrical Hall conductivities σ_{xy} measured in 14 T. (a,b) κ_{xy} of both BiSbTeSe_2 samples change to a positive sign and roughly merge with the corresponding $\sigma_{xy} L_0 T$ above ~ 100 K. (c) For $\text{Bi}_{1.08}\text{Sn}_{0.02}\text{Sb}_{0.9}\text{Te}_2\text{S}$, $\sigma_{xy} L_0 T$ remains below 1% of κ_{xy} , whereas (d) the curves of $\text{Bi}_{1.5}\text{Sb}_{0.5}\text{Te}_{1.7}\text{Se}_{1.3}$ show comparable temperature dependences above ~ 100 K.

ple dependent, whereas low-temperature peaks of negative sign evolve in all four samples with maximum values around -6 mW/Km. In analogy to κ_{xx} , we estimate the expected electronic contribution to the thermal Hall conductivity by using the Wiedemann-Franz law $\kappa_{xy}^{el} = L_0 \sigma_{xy} T$ with the electrical Hall conductivities σ_{xy} measured on the same samples. As shown in Fig. 2, the positive κ_{xy} at higher temperature in both BiSbTeSe_2 samples coincide with hole-dominated electrical Hall conductivities and the estimated κ_{xy}^{el} are of similar magnitude as the measured κ_{xy} . In $\text{Bi}_{1.5}\text{Sb}_{0.5}\text{Te}_{1.7}\text{Se}_{1.3}$, σ_{xy} is electron-like at all temperatures and the obtained κ_{xy}^{el} remains significantly smaller than κ_{xy} , but the temperature dependencies of both quantities become quite similar above ~ 100 K, whereas the obtained κ_{xy}^{el} for $\text{Bi}_{1.08}\text{Sn}_{0.02}\text{Sb}_{0.9}\text{Te}_2\text{S}$ remains below 1% of κ_{xy} up to the highest temperature. Thus we conclude that towards higher temperature thermally excited mobile charge carriers contribute to the THE in samples with a comparatively low excitation gap and a low resistivity. This contribution is weaker in $\text{Bi}_{1.5}\text{Sb}_{0.5}\text{Te}_{1.7}\text{Se}_{1.3}$ with an overall enhanced resistivity signalling a reduced mobility of charge carriers, and becomes negligible in $\text{Bi}_{1.08}\text{Sn}_{0.02}\text{Sb}_{0.9}\text{Te}_2\text{S}$ that is the best compensated TI with a very large excitation gap. The different behavior of mobile charge carriers in these samples is also reflected in different magnetic-field dependencies of the electrical

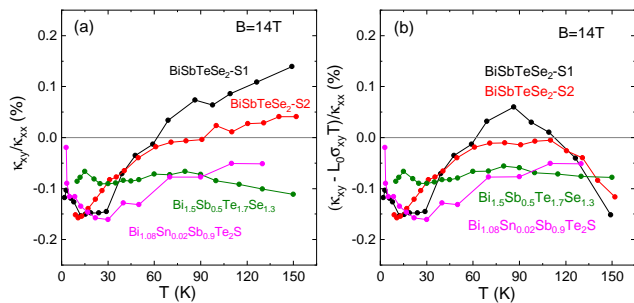


FIG. 3. Temperature dependent thermal Hall ratio obtained by using either (a) the total κ_{xy} or (b) the estimated phonon Hall thermal conductivity $\kappa_{xy} - L_0\sigma_{xy}T$. The correction in (b) leaves the data of the three better conducting samples practically unchanged up to ~ 60 K, and for $\text{Bi}_{1.08}\text{Sn}_{0.02}\text{Sb}_{0.9}\text{Te}_2\text{S}$ this holds in the entire temperature range.

Hall effect, which in all samples becomes non-linear below about 100 K, see appendix, but these differences are not in the focus of this report.

The central result of this study concerns the large low-temperature THE presenting a low-temperature peak of κ_{xy} , which is orders of magnitude larger than what could be conventionally explained to arise from mobile charge carriers, see Fig. 2. This low-temperature peak is a common feature of all four samples despite pronounced differences concerning their electrical (Hall) conductivities, which further supports that the underlying mechanism of the low-temperature thermal Hall effect is not related to the mobile charge carriers. A natural candidate for a common mechanism is the almost identical phonon heat conductivity and in fact the peak of κ_{xy} at 10–14 K is located close to the corresponding peak of κ_{xx} occurring at 8–12 K, see Fig. 1(b,e). Analogous peak coincidences of κ_{xx} and κ_{xy} have been reported for various insulating materials over the last years and are discussed as characteristic indicators of a THE that is generated by phonons [16, 26, 33]. A common feature of those materials is a large thermal Hall angle that is expressed by the peak ratios $|\kappa_{xy}|/\kappa_{xx}$, which are typically in the range of 10^{-3} even when the longitudinal κ_{xx} values of the different materials differ by up to three orders of magnitude [14, 16, 17, 33–35].

As shown in Fig. 3, the low-temperature ratio κ_{xy}/κ_{xx} of each of the four compensated TIs is close to -10^{-3} and varies rather weakly in the temperature range below ~ 50 K where the individual peaks of κ_{xy} and κ_{xx} evolve. Thus, the pronounced THE in these TI materials fulfill the above criteria that indicate a phononic origin. In this context, it is also important to mention that these TI samples are nonmagnetic in nature, which rules out the possibility of a low-temperature THE originating from magnons. However, what kind of phononic mechanisms could be capable of generating a THE?. According to a recent theoretical proposal [26], the presence of charged defects in insulators can induce a significant skew scattering of phonons that is linear in magnetic field as a

result of an interference between Rayleigh and Lorentz scattering terms and should be observed in the temperature range around and above the phonon maximum of $\kappa_{xx}(T)$. Considering oxide-based insulators, the authors estimate that oxygen vacancies can induce a chirality κ_{xy}/κ_{xx} of phonon transport of order -10^{-3} that agrees well with our experimental results on the TI materials, but it is also pointed out that the magnitude and even the sign of the expected chirality depend on the relative strength of elastic and attenuation constants [26]. Thus, the above agreement should not be overinterpreted, but the proposed mechanism of a field-linear skew scattering of phonons resulting from charged defects remains a possible source to explain the phonon-related large THE in these TI materials. The occurrence of charged defects in these TIs is naturally expected from the charge compensation that works in such a way that additional acceptors bind the extra electrons coming from donors, which results in negatively charged occupied acceptors and positively charged empty donors. In order to reach insulating bulk behavior, donor and acceptor densities need to be adjusted properly [28] and a particular feature of these charge-compensated TI materials is the occurrence of self-organized charge puddles in the low-temperature range [36]. The size and connectivity of charge puddles can drastically change the DC electrical resistance and cause characteristic frequency dependences of the AC conductivities in the microwave to infrared range [37, 38]. As such effects also influence the screening of charged defects, they can also be relevant for the proposed skew-scattering mechanism of phonons to induce a large THE in insulators.

To conclude, we have conducted a comparative study of thermal and charge transport in various single crystals of charge compensated TIs. Our key result concerns field-linear thermal Hall conductivity κ_{xy} in all these samples, which becomes most pronounced below about 60 K and peaks around 10 K, where the longitudinal $\kappa_{xx}(T)$ shows the typical maximum of phonon-dominated heat transport. The corresponding thermal Hall ratios are extraordinarily large $\kappa_{xy}/\kappa_{xx} \sim -10^{-3}$ and vary little between the samples and over the temperature range where the TIs remain insulating. In this respect, the compensated TIs behave similar to various ionic insulators for which a large THE of phononic origin has been reported [14, 16, 17, 33–35]. A skew scattering of phonons induced by charged defects has been suggested as underlying mechanism of a phononic THE in those ionic insulators [26], and a similar mechanism could be relevant in these TIs, because the insulating bulk behavior requires charge compensation that naturally induces charged defects via occupied acceptors and empty donors.

ACKNOWLEDGMENTS

We thank A. Rosch, J. Hemberger and G. Grissonanhe for helpful discussions. We acknowledge support

-
- [1] Y. Kasahara, T. Ohnishi, Y. Mizukami, O. Tanaka, S. Ma, K. Sugii, N. Kurita, H. Tanaka, J. Nasu, Y. Motome, *et al.*, *Nature* **559**, 227 (2018).
- [2] C. Strohm, G. L. J. A. Rikken, and P. Wyder, *Phys. Rev. Lett.* **95**, 155901 (2005).
- [3] L. Sheng, D. N. Sheng, and C. S. Ting, *Phys. Rev. Lett.* **96**, 155901 (2006).
- [4] T. Qin, J. Zhou, and J. Shi, *Phys. Rev. B* **86**, 104305 (2012).
- [5] M. Mori, A. Spencer-Smith, O. P. Sushkov, and S. Maekawa, *Phys. Rev. Lett.* **113**, 265901 (2014).
- [6] T. Ideue, Y. Onose, H. Katsura, Y. Shiomi, S. Ishiwata, N. Nagaosa, and Y. Tokura, *Phys. Rev. B* **85**, 134411 (2012).
- [7] Y. Onose, T. Ideue, H. Katsura, Y. Shiomi, N. Nagaosa, and Y. Tokura, *Science* **329**, 297 (2010).
- [8] M. Hirschberger, R. Chisnell, Y. S. Lee, and N. P. Ong, *Phys. Rev. Lett.* **115**, 106603 (2015).
- [9] H. Zhang, C. Xu, C. Carnahan, M. Sretenovic, N. Suri, D. Xiao, and X. Ke, *Phys. Rev. Lett.* **127**, 247202 (2021).
- [10] T. Ideue, T. Kurumaji, S. Ishiwata, and Y. Tokura, *Nature Materials* **16**, 797 (2017).
- [11] G. Grissonnanche, A. Legros, S. Badoux, E. Lefrançois, V. Zlatko, M. Lizaïre, F. Laliberté, A. Gourgout, J. S. Zhou, S. Pyon, T. Takayama, H. Takagi, S. Ono, N. Doiron-Leyraud, and L. Taillefer, *Nature* **571**, 376 (2019).
- [12] G. Grissonnanche, S. Thériault, A. Gourgout, M. E. Boulanger, E. Lefrançois, A. Ataei, F. Laliberté, M. Dion, J. S. Zhou, S. Pyon, T. Takayama, H. Takagi, N. Doiron-Leyraud, and L. Taillefer, *Nature Physics* **16**, 1108 (2020).
- [13] K. Sugii, M. Shimozawa, D. Watanabe, Y. Suzuki, M. Halim, M. Kimata, Y. Matsumoto, S. Nakatsuji, and M. Yamashita, *Phys. Rev. Lett.* **118**, 145902 (2017).
- [14] M.-E. Boulanger, G. Grissonnanche, S. Badoux, A. Llaïre, É. Lefrançois, A. Legros, A. Gourgout, M. Dion, C. H. Wang, X. H. Chen, R. Liang, W. N. Hardy, D. A. Bonn, and L. Taillefer, *Nature Communications* **11**, 5325 (2020).
- [15] T. Uehara, T. Ohtsuki, M. Udagawa, S. Nakatsuji, and Y. Machida, *Nature Communications* **13**, 4604 (2022).
- [16] L. Chen, M.-E. Boulanger, Z.-C. Wang, F. Tafti, and L. Taillefer, *Proceedings of the National Academy of Science* **119**, e2208016119 (2022).
- [17] X. Li, B. Fauqué, Z. Zhu, and K. Behnia, *Phys. Rev. Lett.* **124**, 105901 (2020).
- [18] S. Sim, H. Yang, H.-L. Kim, M. J. Coak, M. Itoh, Y. Noda, and J.-G. Park, *Phys. Rev. Lett.* **126**, 015901 (2021).
- [19] S. Jiang, X. Li, B. Fauqué, and K. Behnia, *Proceedings of the National Academy of Science* **119**, e2201975119 (2022).
- [20] X. Li, Y. Machida, A. Subedi, Z. Zhu, L. Li, and K. Behnia, *Nature Communications* **14**, 1027 (2023).
- [21] L. Mangeolle, L. Balents, and L. Savary, *Phys. Rev. B* **106**, 245139 (2022).
- [22] Y. Zhang, Y. Teng, R. Samajdar, S. Sachdev, and M. S. Scheurer, *Phys. Rev. B* **104**, 035103 (2021).
- [23] X. Zhang, Y. Zhang, S. Okamoto, and D. Xiao, *Phys. Rev. Lett.* **123**, 167202 (2019).
- [24] H. Guo, D. G. Joshi, and S. Sachdev, *Proceedings of the National Academy of Science* **119**, e2215141119 (2022).
- [25] H. Guo and S. Sachdev, *Phys. Rev. B* **103**, 205115 (2021).
- [26] B. Flebus and A. H. MacDonald, *Phys. Rev. B* **105**, L220301 (2022).
- [27] Y. Ando, *Journal of the Physical Society of Japan* **82**, 102001 (2013).
- [28] Z. Ren, A. A. Taskin, S. Sasaki, K. Segawa, and Y. Ando, *Phys. Rev. B* **84**, 165311 (2011).
- [29] S. K. Kushwaha, I. Pletikosić, T. Liang, A. Gyenis, S. H. Lapidus, Y. Tian, H. Zhao, K. S. Burch, J. Lin, W. Wang, H. Ji, A. V. Fedorov, A. Yazdani, N. P. Ong, T. Valla, and R. J. Cava, *Nature Communications* **7**, 11456 (2016), arXiv:1508.03655 [cond-mat.str-el].
- [30] J. Navrátil, J. Horák, T. Plecháček, S. Kamba, P. Lošt'ák, J. Dyck, W. Chen, and C. Uher, *Journal of Solid State Chemistry* **177**, 1704 (2004).
- [31] M. Yao, C. Opeil, S. Wilson, and M. Zebarjadi, *MRS Communications* **7**, 922 (2017).
- [32] J. S. Dyck, W. Chen, C. Uher, Č. Drašar, and P. Lošt'ák, *Physical Review B* **66**, 125206 (2002).
- [33] E. Lefrançois, G. Grissonnanche, J. Baglo, P. Lampen-Kelley, J.-Q. Yan, C. Balz, D. Mandrus, S. E. Nagler, S. Kim, Y.-J. Kim, N. Doiron-Leyraud, and L. Taillefer, *Phys. Rev. X* **12**, 021025 (2022).
- [34] M.-E. Boulanger, G. Grissonnanche, E. Lefrançois, A. Gourgout, K.-J. Xu, Z.-X. Shen, R. L. Greene, and L. Taillefer, *Phys. Rev. B* **105**, 115101 (2022).
- [35] R. Hentrich, M. Roslova, A. Isaeva, T. Doert, W. Brenig, B. Büchner, and C. Hess, *Phys. Rev. B* **99**, 085136 (2019).
- [36] N. Borgwardt, J. Lux, I. Vergara, Z. Wang, A. A. Taskin, K. Segawa, P. H. M. van Loosdrecht, Y. Ando, A. Rosch, and M. Grüninger, *Phys. Rev. B* **93**, 245149 (2016).
- [37] O. Breunig, Z. Wang, A. A. Taskin, J. Lux, A. Rosch, and Y. Ando, *Nature Communications* **8**, 15545 (2017).
- [38] M. Bagchi, L. Pitz-Paal, C. P. Grams, O. Breunig, N. Borgwardt, Z. Wang, Y. Ando, M. Grüninger, and J. Hemberger, *Phys. Rev. B* **99**, 161121 (2019).
-

Appendix A: Electrical Hall versus thermal Hall effect in topological insulators

Figure 4 gives an overview of the magnetoresistance and the electrical Hall ratio of the four compensated TIs. At stabilized temperatures and constant magnetic fields, the Hall resistivity $\rho_{yx}(B)$ and the longitudinal resistivity $\rho_{xx}(B)$ were obtained by, respectively, anti-symmetrizing and symmetrizing the corresponding transverse (U_y) and longitudinal (U_x) voltages measured in the field range up to ± 14 T. As seen in panels (a–d), the normalized magnetoresistance is large in all samples ranging from several 10% in BiSbTeSe₂ and Bi_{1.5}Sb_{0.5}Te_{1.7}Se_{1.3} to a factor of 3 in Bi_{1.08}Sn_{0.02}Sb_{0.9}Te₂S. The Hall ratios, shown in (e–f), reach values up about 30%, but are of different signs depending on the sample and/or the temperature. Generally, the Hall ratios show non-linear field dependencies at low temperatures and approach field-linear behavior towards higher temperature.

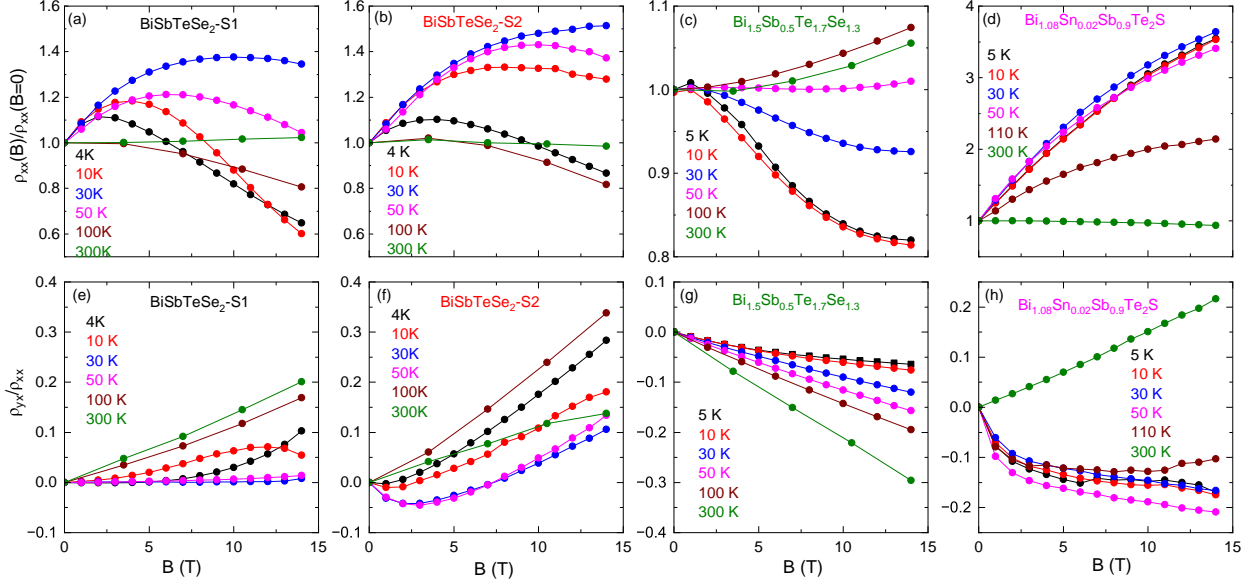


FIG. 4. (a–d) Normalized resistivity $\rho_{xx}(B)/\rho_{xx}(B=0)$ and (e–h) Hall ratio $\rho_{yx}(B)/\rho_{xx}(B)$ of charge-compensated TIs.

From $\rho_{xx}(B)$ and $\rho_{yx}(B)$ the electrical Hall conductivity $\sigma_{xy}(B) = \rho_{yx}/(\rho_{xx}^2 + \rho_{yx}^2)$ is calculated, from which we estimate the electronic contribution to the thermal Hall conductivity $\kappa_{xy}^{el}(B) = L_0 \sigma_{xy}(B) T$ by using the Wiedemann-Franz law with temperature T and Lorenz number $L_0 \approx 2.44 \times 10^{-8} \text{ V}^2 \text{ K}^{-2}$. In Figs. 5–8, the Hall resistivities $\rho_{yx}(B)$ are shown in the left panels while the obtained $\kappa_{xy}^{el}(B)$ are displayed in the middle panels and can be compared to the measured total thermal Hall conductivities $\kappa_{xy}(B)$ shown in the right panels. As discussed in the main text, in all four samples the longitudinal thermal conductivities κ_{xx} vary by less than 2% up to a magnetic field of 14 T, see Fig. 1(c), and the thermal Hall conductivities κ_{xy} remain field-linear over the entire temperature range.

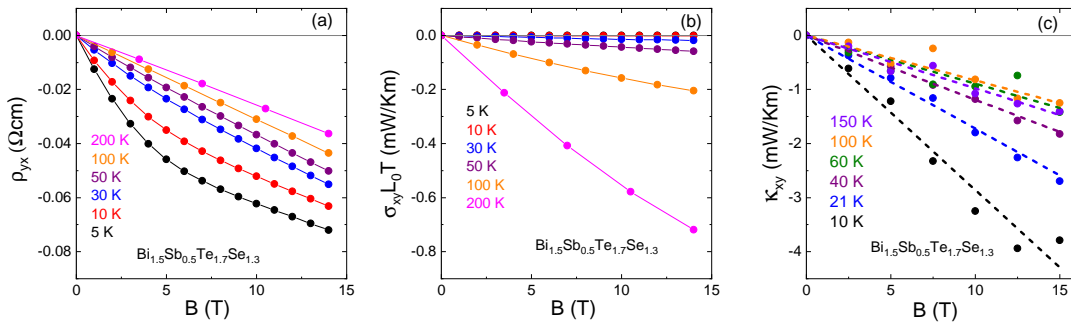


FIG. 5. (a) Hall resistivity $\rho_{yx}(B)$ and (b) the corresponding electronic contribution to the thermal Hall conductivity $\kappa_{xy}^{el}(B)$ in comparison to (c) the measured total Hall conductivity $\kappa_{xy}(B)$ of Bi_{1.5}Sb_{0.5}Te_{1.7}Se_{1.3}. The dashed lines in (c) are linear fits that were used to calculate the temperature dependent $\kappa_{xy}(T)$ at constant fields (see text).

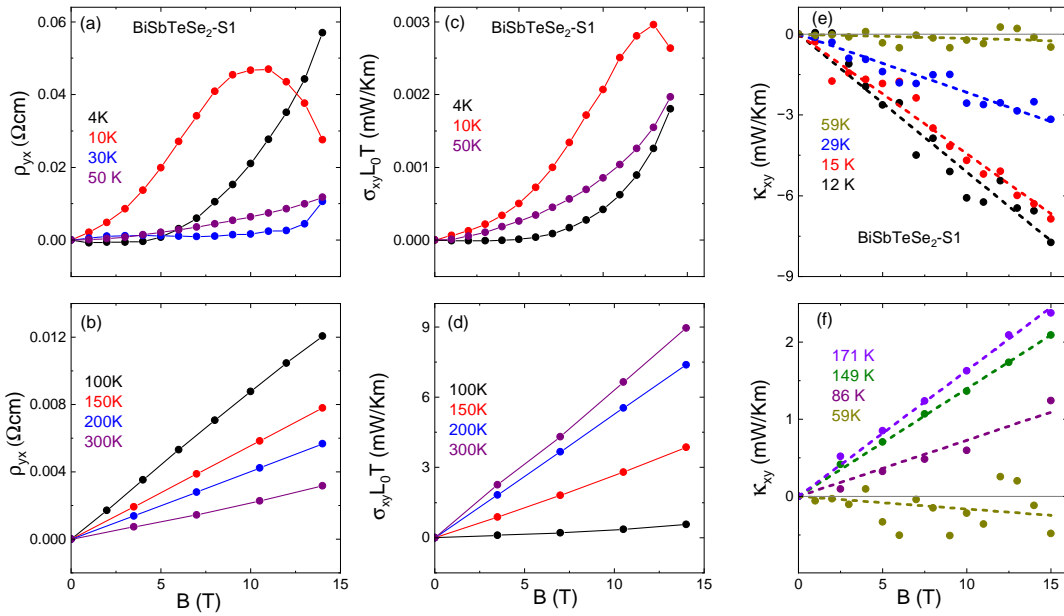


FIG. 6. (a,b) Hall resistivity $\rho_{yx}(B)$ and (c,d) the corresponding electronic contribution to the thermal Hall conductivity $\kappa_{xy}^{el}(B)$ in comparison to (e,f) the measured total Hall conductivity $\kappa_{xy}(B)$ of BiSbTeSe₂ (sample 1). The dashed lines in (e,f) are linear fits that were used to calculate the temperature dependent $\kappa_{xy}(T)$ at constant fields (see text).

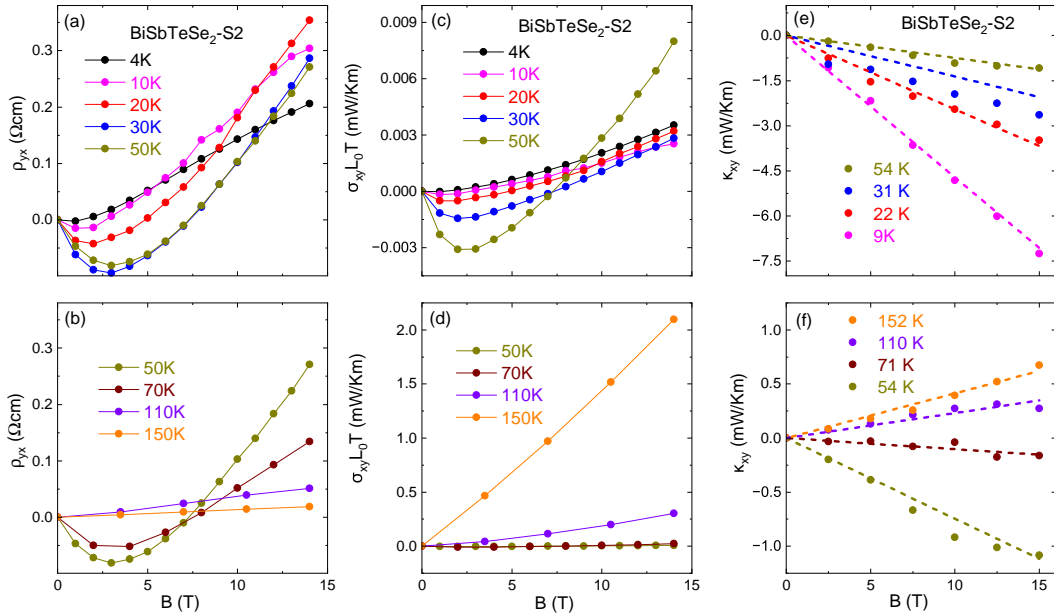


FIG. 7. (a,b) Hall resistivity $\rho_{yx}(B)$ and (c,d) the corresponding electronic contribution to the thermal Hall conductivity $\kappa_{xy}^{el}(B)$ in comparison to (e,f) the measured total Hall conductivity $\kappa_{xy}(B)$ of BiSbTeSe₂ (sample 2). The dashed lines in (e,f) are linear fits that were used to calculate the temperature dependent $\kappa_{xy}(T)$ at constant fields (see text).

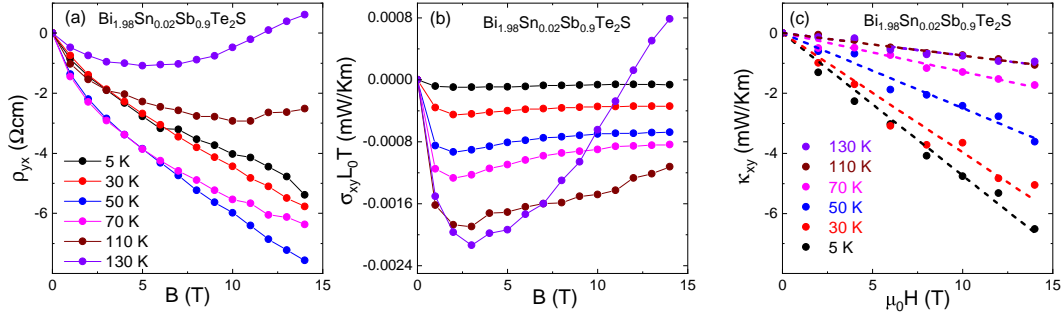


FIG. 8. (a) Hall resistivity $\rho_{yx}(B)$ and (b) the corresponding electronic contribution to the thermal Hall conductivity $\kappa_{xy}^{el}(B)$ in comparison to (c) the measured total Hall conductivity $\kappa_{xy}(B)$ of $\text{Bi}_{1.08}\text{Sn}_{0.02}\text{Sb}_{0.9}\text{Te}_2\text{S}$. The dashed lines in (c) are linear fits that were used to calculate the temperature dependent $\kappa_{xy}(T)$ at constant fields (see text).